



HAL
open science

Reflective filtered backprojection: numerical results

Jean-Baptiste Bellet, Gérard Berginc

► **To cite this version:**

Jean-Baptiste Bellet, Gérard Berginc. Reflective filtered backprojection: numerical results. 2015.
hal-01207522

HAL Id: hal-01207522

<https://hal.science/hal-01207522>

Preprint submitted on 1 Oct 2015

HAL is a multi-disciplinary open access archive for the deposit and dissemination of scientific research documents, whether they are published or not. The documents may come from teaching and research institutions in France or abroad, or from public or private research centers.

L'archive ouverte pluridisciplinaire **HAL**, est destinée au dépôt et à la diffusion de documents scientifiques de niveau recherche, publiés ou non, émanant des établissements d'enseignement et de recherche français ou étrangers, des laboratoires publics ou privés.

REFLECTIVE FILTERED BACKPROJECTION: NUMERICAL RESULTS

JEAN-BAPTISTE BELLET AND GÉRARD BERGINC

ABSTRACT. This paper gives new insights on reflective tomography. It provides original numerical results both in 2D and 3D. They show that using the filtered backprojection on reflective images is a sensitivity analysis. By combination of the contrasts of the original images, this approach constructs indeed a volume whose most intense voxels are located near the surfaces of the original scene. Thus the combination of the FDK algorithm with the Maximum Intensity Projection is very relevant to generate new views of the considered scene. On numerical examples, we investigate the effect of the input contrasts, we show the robustness with respect to angle-dependancy and we show the stability. We also apply the method for a recognition problem from optronic images.

Keywords. Reflective tomography, FDK algorithm, Maximum Intensity Projection, optronic recognition

1. INTRODUCTION

The Radon transform encounters a great success in several communities. In X-Ray tomography, since transmission models involve the Radon transform, numerical reconstruction of media are provided by inversion of the Radon transform [1], and especially by filtered backprojection (FBP). In pattern recognition the Hough transform for detection of linear features is similar to the adjoint of the Radon transform. By the way the direct use of FBP has been extended to different kind of imaging modalities. In particular the use of FBP on reflective-kind images, including images of backscattered intensity, is a heuristics which provides interesting reconstruction results [2, 3]. This heuristics is the so-called reflective tomography. We can more particularly distinguish a 3D laser imaging technique which is emerging [4, 3, 5, 6, 7]. This method is very promising, in particular in the field of target recognition: using a set of 2D images of occluded objects, it enables automatic real-time 3D visualization of the scene, and 3D extraction of targets [8].

To understand the heuristics of reflective tomography from a mathematical point of view, we have proposed an original mathematical study in [9], where the effect of FBP on some general model of reflective images is mathematically formulated. We have considered a scene with opaque objects which generates piecewise smooth projections. We have expressed the FBP of such projections in function of the variations and the jumps of the recorded images. We have emphasized that this constitutes some sensitivity analysis; it constructs a volume where the most intense voxels must be generically located near the surfaces of the scene that generate coherent variations in the recorded images.

In this paper we provide original numerical results of the reflective filtered backprojection. We first study a 2D case. We recall the main results of [9] without the technical details, and, step by step, we illustrate the reflective projection, the tomographic filtering of such data, and the associated filtered backprojection. We emphasize where coherence occurs in the filtered sinogram, and thus why the most intense values in the reconstruction are generically located near the surfaces of the scene. Then we consider the 3D extension which uses the famous FDK algorithm [10, 1]. We illustrate this process step by step. We recall a 3D visualization principle which is very efficient for a reflective FDK volume: the Maximum Intensity Projection (MIP) [11, 8]. We show that the sequence FDK-MIP is relevant for reflective images. We provide several examples which correspond to different explanations of contrasts. They confirm the role of the variations, and show for example that tangential contributions enable the reconstruction of pieces which are invisible on a binary dataset. We then propose a robustness test; we show that the method does not need any particular assumption about the dependance of data with respect to the angles of projection: the method successully recombines coherent contrasts of the dataset, even if changes in the direct problem appear. We show the stability of the process: we test the effect of additive noise and the effect

of speckle noise, for several orders of magnitude of noise. To conclude, we apply the process on optronic data; it shows the interest of the method for the recognition problem from optronic images.

2. 2D STUDY

In the plane \mathbb{R}^2 , we consider a set of curves $(\Sigma_i)_{1 \leq i \leq n}$, inside a curve Σ_0 . Σ_0 plays the role of the wall of the experiment, whereas the Σ_i , $1 \leq i \leq n$, play the role of opaque objects. We consider a screen of projection which is oriented along a unitary vector $\theta \in S^1$. Each point of the screen belongs to a line which is orthogonal to θ : $x \cdot \theta = s$, which plays the role of a line of projection. At such a point, we measure an information $f(y(\theta, s), \theta)$, which comes from a point of the scene: $y(\theta, s) \in \cup_{0 \leq i \leq n} \Sigma_i$, along the line of projection: $y(\theta, s) \cdot \theta = s$. The opacity assumption means that $y(\theta, s)$ is the first intersection point of the line with the objects. On the screen, we then get a 1D-projection $F_\theta : s \mapsto f(y(\theta, s), \theta)$. Eventually but not necessary, f can represent a light intensity which is backscattered after an illumination of the scene. That is the reason why use the terminology of *reflective* projection; also we sometimes call f the emission *intensity*. An example of reflective projection F_θ is represented on the Figure 1. We have represented a scene with three objects: rectangle, bucket, banana, inside a circular wall. A projection on a screen is represented: the edges of projection, which join screen pixels with the points of emission $y(\theta, s)$ have been drawn; the gray level of an edge is the value of the projected intensity. It is reasonable to assume that the projection F_θ is piecewise smooth. On the example, the represented projection contains portions of objects which belong successively to: wall, rectangle, wall, bucket, banana, wall. There is a jump at every interface. There is also a jump on the bucket. Outside these jumps, the image is smooth. Let us mention that if the screen were vertical and on the right, there would be a jump on the concavity of the banana. The process is repeated for a finite number of angles: θ scans a finite set $\Theta \subset S^1$. Thus we get a *reflective sinogram*: $F : (\theta, s) \mapsto F_\theta(s)$, which is the juxtaposition of the individual projections F_θ , $\theta \in \Theta$. For the considered example, θ scans a full circle, with a step of one degree. The dataset is represented on Figure 1, on the right.

The first step of the reconstruction algorithm is applying a tomographic filtering on each individual projection F_θ . We get from the jumps formula:

$$\partial_s F_\theta \star \varphi(s) = \int_{\Sigma(\theta)} \partial_\tau f(y, \theta) \varphi(s - y \cdot \theta) d\sigma(y) + \sum_j [f_{\theta, j}] \varphi(s - s(\theta, j)).$$

Here, $\Sigma(\theta) := \{y(\theta, s), s\}$ denotes the visible part of the scene, $\partial_\tau f(\cdot, \theta)$ is the tangential derivative of $f(\cdot, \theta)$ on $\Sigma(\theta)$, and the jumps of F_θ are the $[f_{\theta, j}]$, located at the $s(\theta, j)$. The filter φ is a low-pass version of the Hilbert kernel; in particular φ is odd, and the size of its main lobe is proportional to the inverse of its maximum frequency. Filtering of each projection in the sinogram yields a filtered sinogram: see Figure 2, on the left. Because of the effect of the derivative and the shape of φ , the variations and the jumps from the original projections are emphasized. In particular a contour detection (jumps) of zero-crossing type can be noticed.

The next step is backprojecting the filtered sinogram. For instance the image of the first example has been filtered and then backprojected: see Figure 2, on the right. We see again that the variations and the jumps of the original projection are emphasized. Superposing the backprojection of each filtered image yields the final FBP, which is represented on Figure 3. The main parts of the scene that are reconstructed are those where the intensity varies, such as the concavity of the banana, and the points whose intensity are located near jumps for some angles, such as the North-East corner of the rectangle. This is consistent with the following analysis. The mathematical expression of this reconstruction by FBP is deduced from the expression of the filtered sinogram:

$$\mathcal{R}^*[\partial_s F_\theta \star \varphi](x) = \sum_{\theta \in \Theta} \left[\int_{\Sigma(\theta)} \partial_\tau f(y, \theta) \varphi((x - y) \cdot \theta) d\sigma(y) + \sum_j [f_{\theta, j}] \varphi(x \cdot \theta - s(\theta, j)) \right].$$

Here, \mathcal{R}^* denotes the adjoint of the Radon transform, which sums over lines through x : $\mathcal{R}^*[g](x) = \sum_{\theta \in \Theta} g(x \cdot \theta)$. For every pixel x of the reconstruction, the computed value is the sum along the sinusoid $x \cdot \theta = s$ in the filtered sinogram. A point of the scene: $y \in \cup_i \Sigma_i$ is visible in the sinogram along a piece of the curve $y \cdot \theta = s$: see Figure 1. Then y is essentially visible in the filtered sinogram in a neighborhood of this piece, with an intensity level which depends on the contrasts at y in the dataset. For x close to y , a piece of the sinusoid $x \cdot \theta = s$ can contain coherent data in the filtered

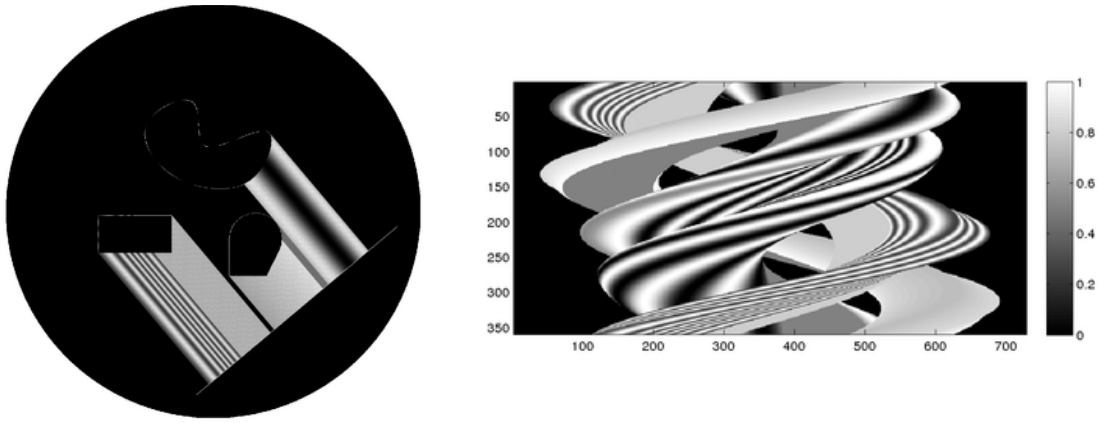


FIGURE 1. One projection on a screen inside a circular wall (on the left) and a reflective sinogram (on the right): juxtaposition of the collected projections.

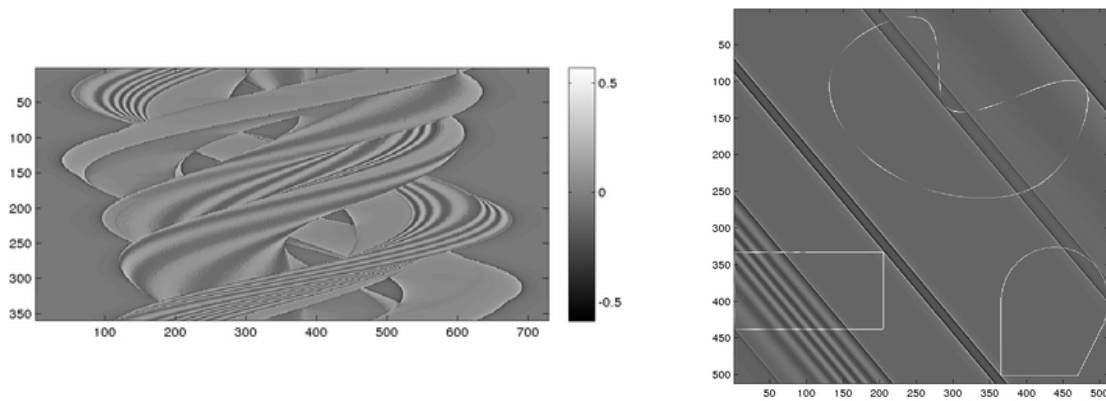


FIGURE 2. On the left: filtered sinogram. On the right: backprojection of a single filtered projection. Filtering emphasizes the variations and the jumps.

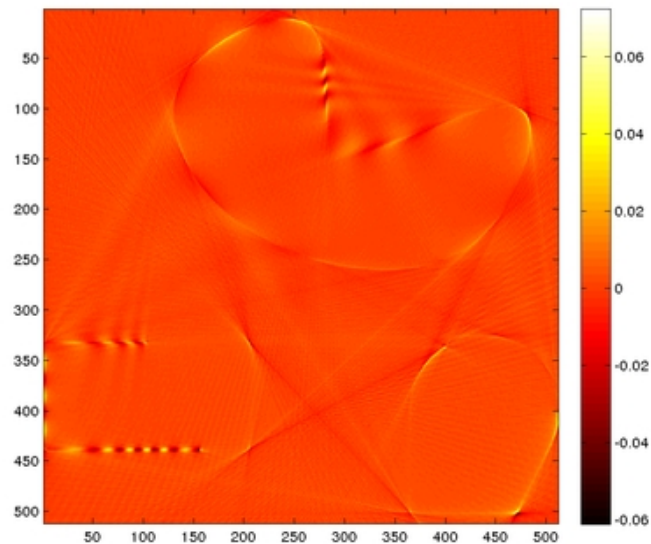


FIGURE 3. FBP over the whole sinogram superposes the backprojection of the filtered projections.

sinogram: see Figure 2. Such coherent data are constructively added by summation, and thus give a significant contribution at x . Of course the value of this significant contribution depends on the intensity levels of the coherent data, and depends also on the angular range of visibility of y . By the way, along a generical sinusoid $x \cdot \theta = s$, where x is far from $\cup_i \Sigma_i$, the filtered data are incoherent and thus summing along such a sinusoid yields a value which is generically low.

3. 3D EXTENSION

We now consider the 3D extension of the 2D reflective filtered backprojection: we use the FDK algorithm to compute a 3D reconstruction, from 2D reflective images of a cone-beam scanning experiment. We take perspective projections of a scene, by turning horizontally around it. On the Figure 4, we have represented some views of a sequence of 360 images, one degree step. The first step of the FDK algorithm is applying horizontally the tomographic filtering; this especially emphasizes the horizontal variations, including the contours which are transverse to the horizontal direction: see Figure 4. Also juxtaposing the different images provides a sinogram: see Figure 5. The next step of the FDK algorithm is the backprojection. For each point of the volume of reconstruction, which is voxelized, an integration over lines through the point is computed; this is done by a summation along a curve in the filtered sinogram. For a generical point, this curve contains incoherent data. But for a point which is close to a surface of the original scene, the curve may contain coherent data that are generated by the contrasts of the input images; such coherent data can be constructively added and enables to obtain a high value at the considered voxel. We have represented slices of the FDK volume for the considered example on the Figure 6. We present below another way of visualization with which it will be easy to identify 3D structures.

We have emphasized that a reflective FDK volume is a 3D volume of sensitivity; the most intense voxels must be located near the surfaces of the original scene. So we use the Maximum Intensity Projection (MIP) to visualize a reflective FDK volume [8]: the volume is projected onto a screen, by selection of the most intense voxel along each ray of projection. This method tries to visualize surfacic points of the original scene; whereas the artifacts tend to become invisible, due to the selection process. The MIP produces efficiently and fastly high contrasted images: see Figure 7 for several angles of view. These results validate the sequence FDK-MIP for 2D reflective images. The object is successfully visualized in 3D with this process; we get semi-transparent representations. The 3D reconstruction allows to compute as many views as required, including views of extracted sub-volumes.

4. NUMERICAL TESTS

4.1. Contrasts. We have represented four examples of reconstruction in the Figure 8. They correspond to different explanations of the contrasts in the images. The general set-up is the following: we take pictures of a tricycle by turning around it over 360 degrees, with a one degree step. For the first case, we assume that we measure binary images. For the second case, we consider a uniform object, but with some lightening effect; this introduces contrasts on the object. For the third case, we assume that the intensity of the object is non-uniform in space, but is constant in angle: the measure depends on the point but does not depend on the angle. For the last case, we combine the two origins of contrasts: we consider a non-uniform object with a lightening effect. For all of the four cases, we represent four images of the sequences, and a MIP. On these examples, we observe that the combination of the FDK algorithm with the MIP works very well for reflective images. It can support different kind of models, it works here for all the cases. We observe that the variations in intensity in the dataset improve the quality of the result. For instance the interior of the wheels is not recovered for the binary dataset but is recovered for the other cases. Also the input contrasts add contrasts in the visualization of the reconstruction.

4.2. Robustness. In this part, we consider projections which depend on the angle of projection. We would like to show that the method is robust to changes during the acquisition process, including changes in the direct problem when the angle changes. We check that FDK recombines the coherent contrasts. The scene is a cow that we observe over 360 degrees (one degree step, and the rotation is done in the plane $x_3 = 0$). We propose three cases: see Figure 9. For the first case, the color of the cow is fixed, and some lightening effect is fixed. For the second case, the color is fixed, and the lightening effect changes with the angle, with randomized rules. For the last case, the lightening

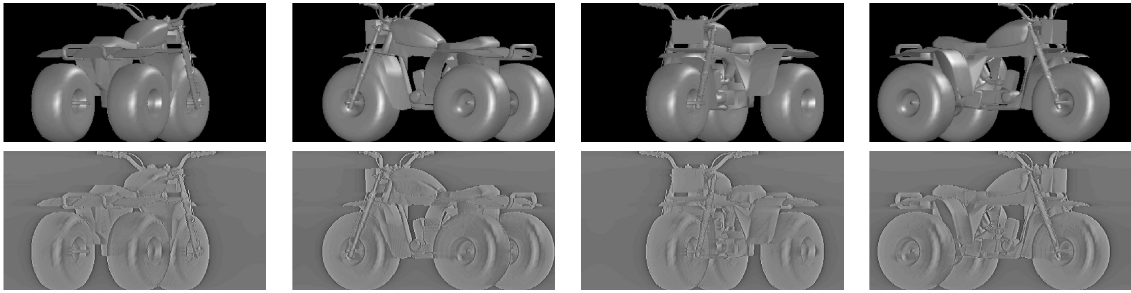


FIGURE 4. Top: reflective images of an object at 60, 150, 240, 330 degrees (from left to right). Bottom: images after horizontal tomographic filtering. Filtering especially emphasizes the horizontal variations, including the jumps.



FIGURE 5. On the left: slices in the reflective sinogram; on the right: slices in the filtered sinogram.

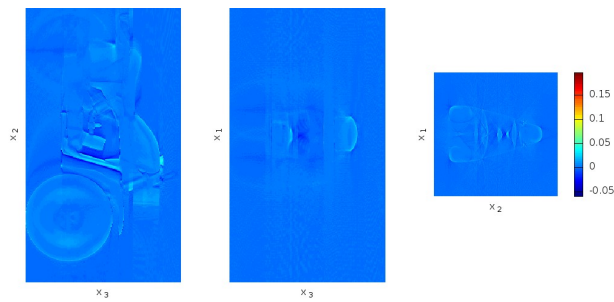


FIGURE 6. Three orthogonal slices in the FDK volume. The most interesting voxels are the most intense ones.

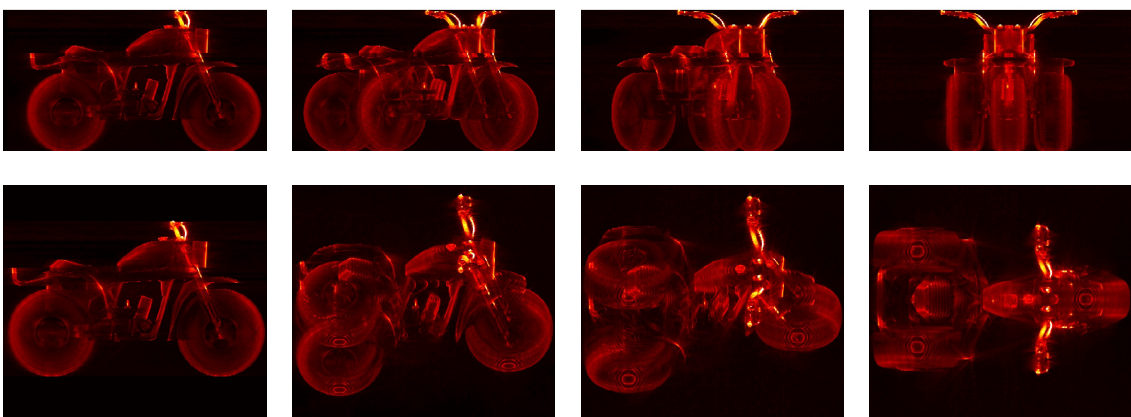


FIGURE 7. MIP views of the reflective FDK volume. Top: rotation in the plane $x_3 = 0$; bottom: rotation in the plane $x_1 = 0$. The sequence FDK-MIP is relevant for reflective images; it successfully generates new semi-transparent views of the scene.

effect is fixed, but the color contains some randomized part. The contrasts of each individual image contain the shape of the object and structures of the body. They depend on the angle, and this dependency becomes more and more severe from the first case to the third one.

For the first two cases, the contrasts tend to be consistent when the angle changes, and so FDK successfully recombines them, and thus the shape and structures of the body are recovered. For the last case, the shape is distinguished on every image; this provides coherent informations that are recombined. But because of the randomization of the color, the contrasts of some structures of the body are not coherent when the angle changes. Their contributions tend to become less significant than the shape contribution in the final reconstruction. We have represented a slice of the filtered sinograms, in the plane $x_3 = 0$: see Figure 10. These slices confirm that the contrast coherency between the images is better for the first two datasets.

To conclude this part, when the intensities depend on the angle, as soon as there are some informations, including structural ones, which remain coherent from image to image, FDK successfully recombines the associated coherent contrasts. In particular the method is robust to slight changes in the direct problem.

4.3. Stability. We consider now a rotation over 360 degrees, one degree step, around a lambertian cow: no variation are due to changes in angle. We get a sinogram d , rescaled to the range $[0, 1]$. But we corrupt the images with an increasing level of noise, $\sigma = 0, 3^{-p}, p = 4, 3, 2, 1, 0$. First we consider additive noise: $d_a = d + \sigma\mathcal{N}(0, 1)$ where $\mathcal{N}(0, 1)$ is the normalized gaussian. And then we consider some speckle noise: $d_s = (1 + d)(1 + \sigma\mathcal{N}(0, 1))$. For each case, we have represented one image of the corrupted sequence, and a MIP of the reconstruction on Figure 11. We observe stability: a small noise in the data introduces a small noise in the reconstruction. By the way, the object can still be quite clearly distinguished in the reconstruction with a noise level of 3^{-1} .

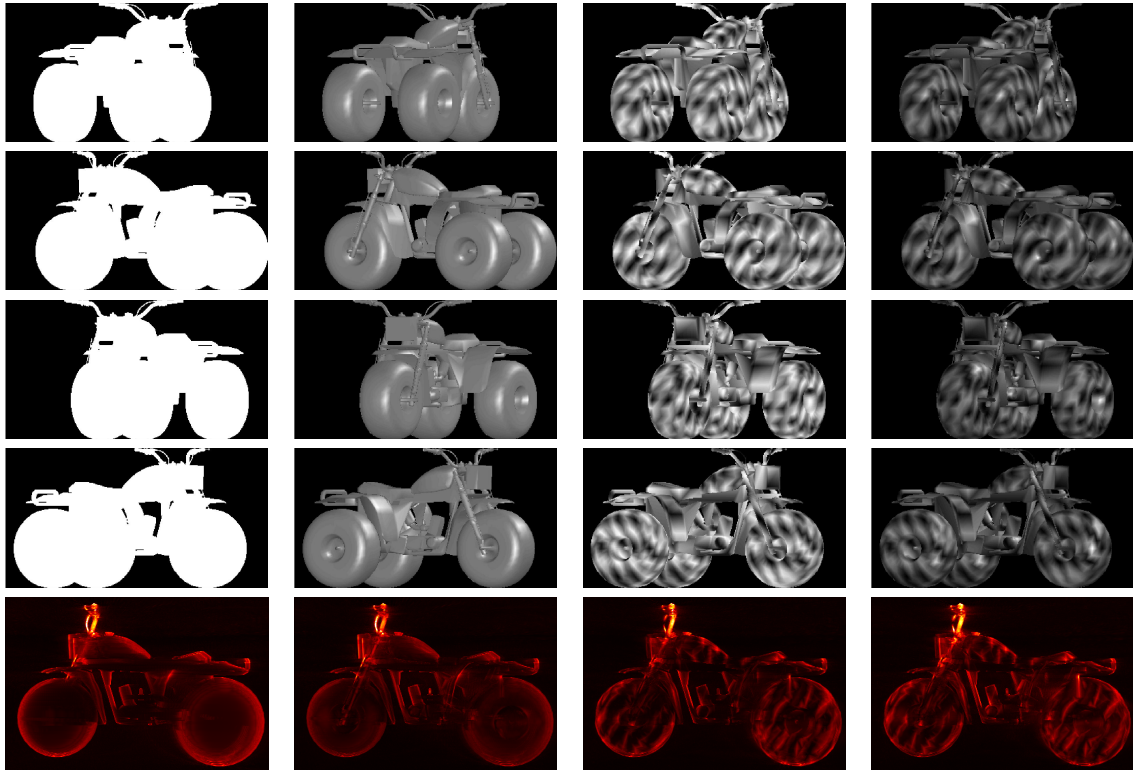


FIGURE 8. From left to right: binary tricycle, uniform tricycle with lightening effect, non-uniform Lambertian tricycle, non-uniform tricycle with lightening effect. From top to bottom: 60, 150, 240, 330 degrees of the original sequence, and a MIP of the reconstruction. Reflective FDK-MIP works, and contrasts improve the quality of the reconstruction.

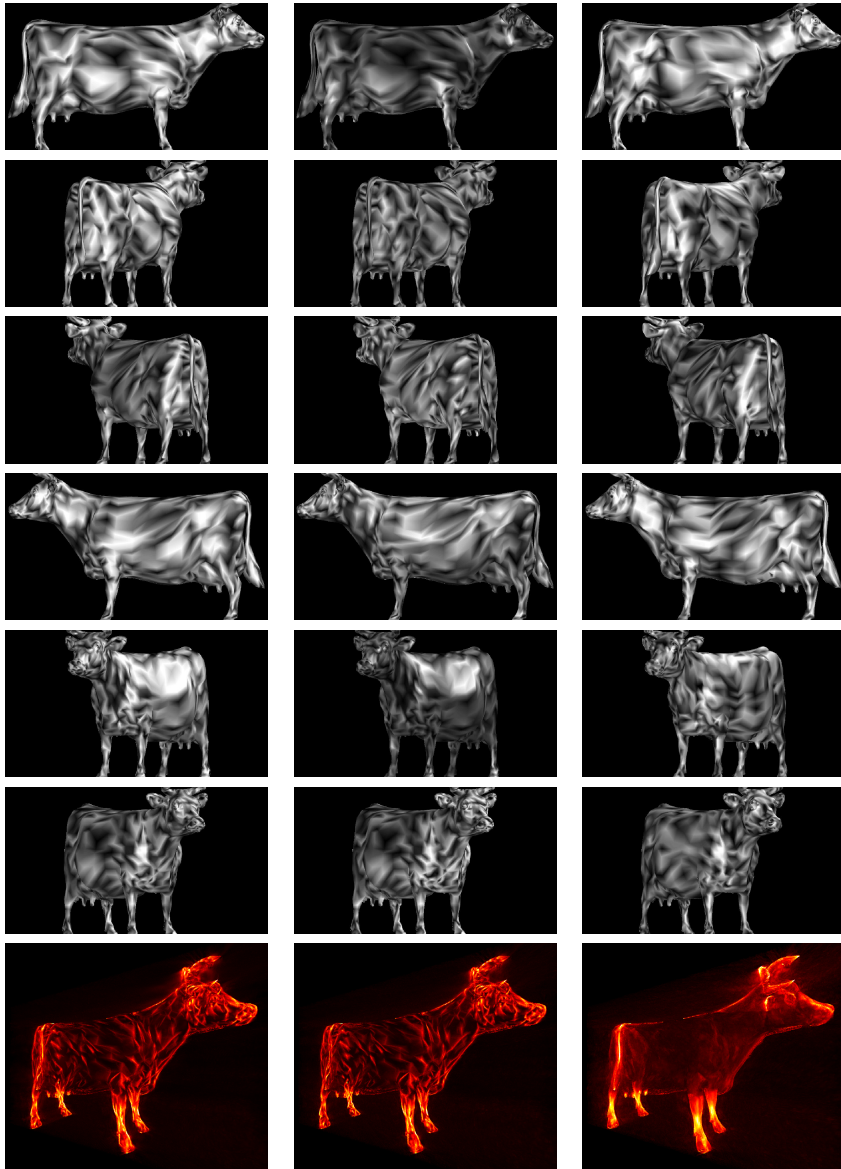


FIGURE 9. Robustness test. From top to bottom: a few images of the sequence, and a MIP of the reconstruction. From left to right: fixed color with fixed lightening effect, fixed color with randomized lightening effect, fixed lightening effect with randomized color. Reflective FDK-MIP recombines the coherent contrasts.

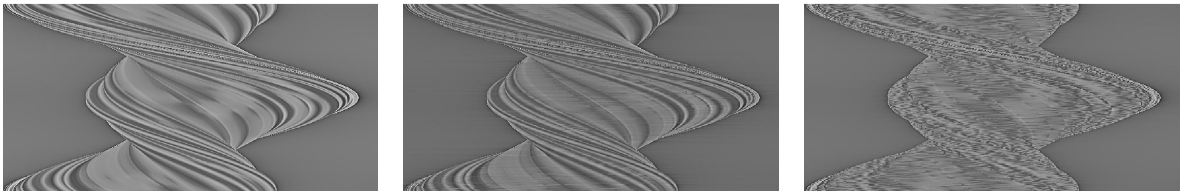


FIGURE 10. Filtered sinograms in the plane $x_3 = 0$ for the datasets of Figure 9. The contrast coherency along sinusoids is better for the first two cases.

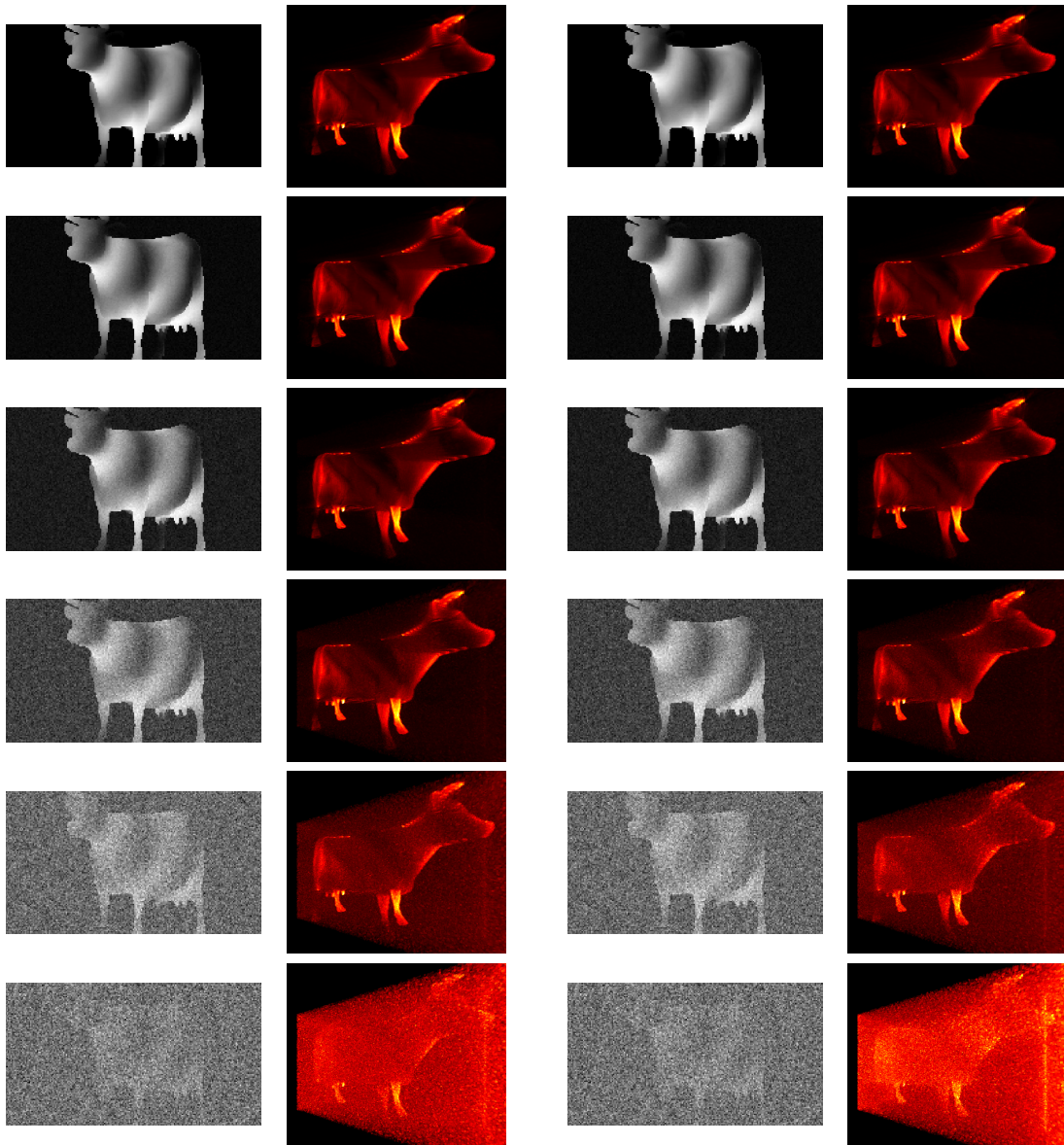


FIGURE 11. From left to right: image with additive noise, associated reconstruction, image with speckle noise, associated reconstruction. From top to bottom: increasing level of noise, $\sigma = 0, 3^{-p}, p = 4, 3, 2, 1, 0$. Reflective FDK-MIP is stable.

5. APPLICATION: OPTRONIC RECOGNITION

In this section we provide an example of using the reflective filtered backprojection in the recognition field. We consider a laser system which provides active laser images of backscattered intensity by rough surfaces. We consider a set of such optronic images, courtesy of Thales Optronics, that has been obtained with a simulated laser system [6]. A sequence of 360 images has been computed by turning around the scene, one degree step. The considered scene is a vehicle behind foliage: see Figure 12 for two samples of the sequence. We apply the FDK-MIP to reconstruct-visualize

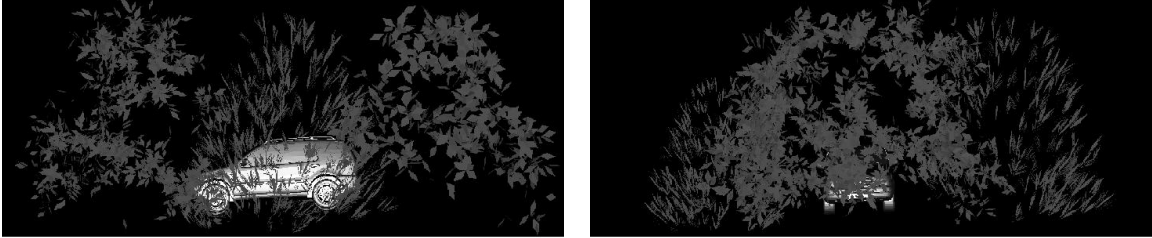


FIGURE 12. Optronic images of a complex scene

the scene. We have represented on Figure 13 such a semi-transparent view of the full scene. We have also represented a view of car, after deletion of the foliage in the reconstructed volume. The method overcomes the difficulties which are generated by the occultations. The extracted car contains features and details that are useful for recognition.

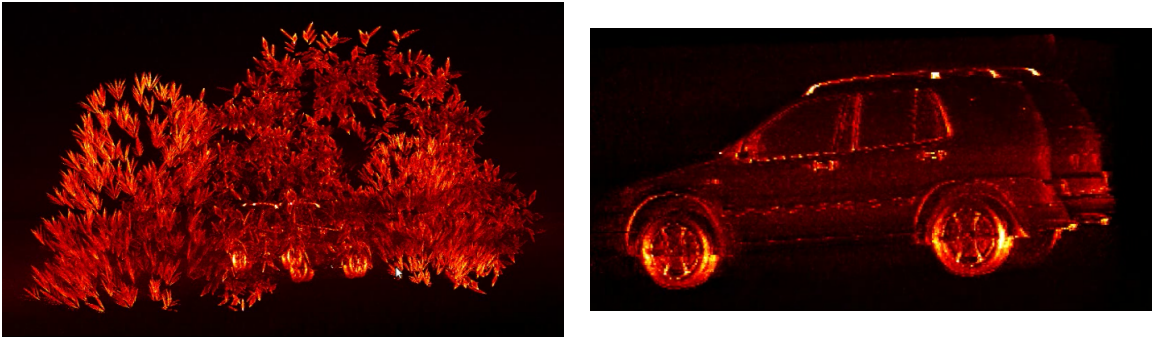


FIGURE 13. Reconstruction of an optronic scene. Full scene (on the left), and after extraction of an interesting sub-volume (on the right).

6. CONCLUSION

The interpretation of the mathematical formulation of reflective tomography is consistent with the numerical results. It provides a new mathematical insight on the subject. The use of FDK on reflective-kind images can be interpreted as a sensitivity analysis which recombines the coherent horizontal contrasts of the dataset, at their true location in space. In particular the MIP is very relevant to visualize a reflective FDK volume. We observe that the sequence FDK-MIP is very stable, and that the method is robust with respect to dependency in angle. We have seen that reflective filtered backprojection works without strong assumption about the *reflection* process, so it is very general and several uses could be imagined. With a binary dataset, we get a reconstruction from shapes. The method can be used for travel-time images. We could imagine two different light sources which illuminate alternately a scene. We have seen a relevant example of target extraction from optronic data. More generally, since active images of backscattered intensity by rough surfaces are coherent and high contrasted, the proposed interpretation shows that the method is very relevant for 3D laser imagery. Finally this paper opens perspectives such as recognition of targets, even when fog, occlusions, or countermeasurements disrupt the acquisition.

REFERENCES

- [1] F. Natterer and F. Wübbeling. *Mathematical methods in image reconstruction*. SIAM, 2007.
- [2] F.K. Knight, S.R. Kulkarni, R.M. Marino, and J.K. Parker. Tomographic Techniques Applied to Laser Radar Reflective Measurements. *Lincoln Laboratory Journal*, 2(2), 1989.
- [3] G. Berginc and M. Jouffroy. Simulation of 3D laser systems. In *Geoscience and Remote Sensing Symposium, 2009 IEEE International, IGARSS 2009*, volume 2, pages 440–444. IEEE, 2009.
- [4] Gérard Berginc and Michel Jouffroy. Optronic system and method dedicated to identification for formulating three-dimensional images. US patent 20110254924 A1, European patent 2333481 A1, FR 09 05720 B1, November 2009.
- [5] G. Berginc and M. Jouffroy. Simulation of 3D laser imaging. *PIERS Online*, 6(5):415–419, 2010.
- [6] G. Berginc and M. Jouffroy. 3D laser imaging. *PIERS Online*, 7(5):411–415, 2011.
- [7] G. Berginc. Scattering models for range profiling and 2D-3D laser imagery. In Leonard M. Hanssen, editor, *Reflection, Scattering, and Diffraction from Surfaces IV, 92050K*, volume 9205 of *Proc. of SPIE*, 2014.
- [8] Jean-Baptiste Bellet, Ion Berechet, Stefan Berechet, Gérard Berginc, and Gaël Rigaud. Laser Interactive 3D Computer Graphics. *2nd International Conference on Tomography of Materials and Structures, Québec*, 2015. <hal-01175855>.
- [9] Jean-Baptiste Bellet and Gérard Berginc. Reflective filtered backprojection. *Submitted*, 2015. <hal-01202974>.
- [10] L.A. Feldkamp, L.C. Davis, and J.W. Kress. Practical cone-beam algorithm. *JOSA A*, 1(6):612–619, 1984.
- [11] J.W. Wallis and T.R. Miller. Three-Dimensional Display in Nuclear Medicine and Radiology. *The Journal of Nuclear Medicine*, 1991.

UNIVERSITÉ DE LORRAINE, INSTITUT ELIE CARTAN DE LORRAINE, UMR 7502, METZ, F-57045, FRANCE,
CNRS, INSTITUT ELIE CARTAN DE LORRAINE, UMR 7502, METZ, F-57045, FRANCE.

E-mail address: jean-baptiste.bellet@univ-lorraine.fr

THALES OPTRONIQUE, 2, AVENUE GAY LUSSAC CS 90502, 78995 ÉLANCOURT CEDEX, FRANCE.

E-mail address: gerard.berginc@fr.thalesgroup.com